Joule

CellPress

Article

Ultrasonic Scanning to Observe Wetting and "Unwetting" in Li-Ion Pouch Cells

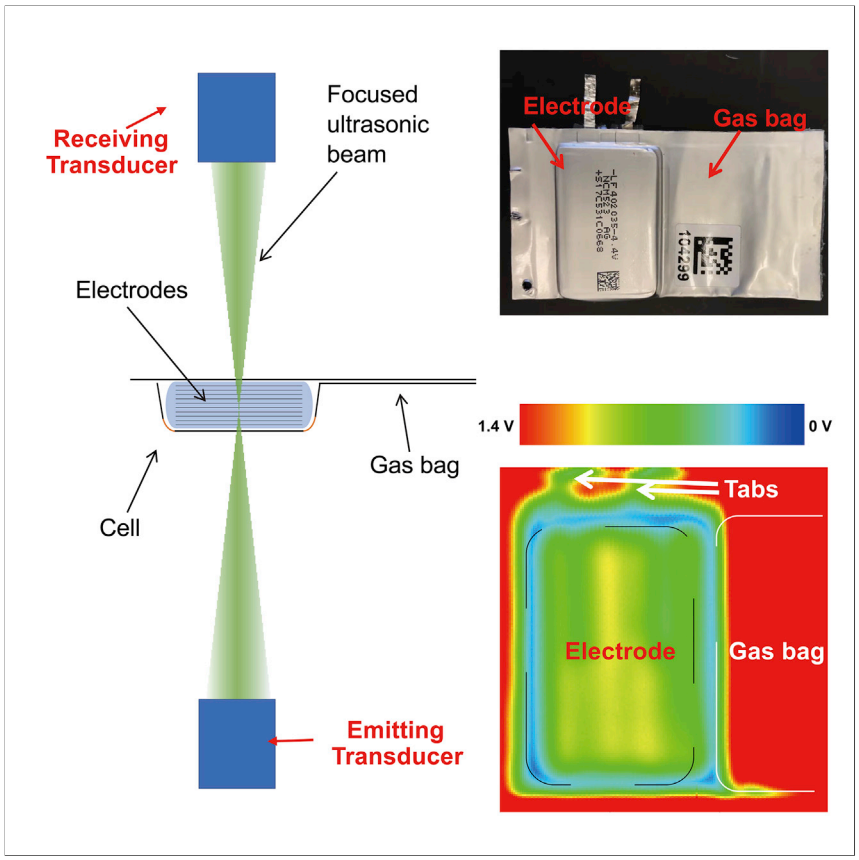

An ultrasonic imaging method is proposed to investigate the quality of electrolyte wetting inside lithium-ion batteries nondestructively. The relationship between battery aging and electrolyte dry-out or "unwetting" is studied with this method.

Zhe Deng, Zhenyu Huang, Yue Shen, ..., Jessie E. Harlow, Roby Gauthier, Jeff R. Dahn

shenyue1213@hust.edu.cn (Y.S.)
huangyh@hust.edu.cn (Y.H.)
jeff.dahn@dal.ca (J.R.D.)

HIGHLIGHTS

Non-destructive ultrasonic imaging of electrolyte wetting

High sensitivity to internal gassing

A quick comparison of electrolyte stability

Deng et al., Joule 4, 2017–2029
September 16, 2020
https://doi.org/10.1016/j.joule.2020.07.014

Joule

CellPress

Article

Ultrasonic Scanning to Observe Wetting and "Unwetting" in Li-Ion Pouch Cells

Zhe Deng,[1,3] Zhenyu Huang,[3] Yue Shen,[1,3,*] Yunhui Huang,[1,3,*] Han Ding,[3,4] Aidan Luscombe,[2] Michel Johnson,[2] Jessie E. Harlow,[2] Roby Gauthier,[2] and Jeff R. Dahn[2,5,*]

SUMMARY

An ultrasonic imaging technique has been developed to investigate the internal changes of pouch cells nondestructively. The local ultrasonic transmittance of pouch cells has been measured and used for imaging with a new ultrasonic scanning machine designed and built in-house. The wetting process of the cells is clearly observed via such ultrasonic imaging techniques. Furthermore, ultrasonic transmission images of fresh cells and aged cells with different electrolytes and cycling conditions exhibit very different ultrasonic transmittance, which can be caused by electrolyte dry-out or "unwetting" due to cell swelling. The ultrasonic imaging technique is a very sensitive method to probe failure mechanisms in Li-ion pouch cells.

INTRODUCTION

Li-ion batteries (LIBs) are the most successful energy storage devices used in mobile electronics, electric vehicles, and large-scale energy storage stations. However, LIBs are still facing challenges in energy density, cycle life, and safety.[1] Recently, many novel characterization methods have been applied in LIB research, which have led to improvements in understanding failure mechanisms and electrochemical performance. However, non-destructive *in-situ* methods that can characterize the internal structure of fully packaged commercial LIBs are still quite rare. X-ray tomography has been used to characterize electrode material structure,[2] geometric parameters,[3] thermal-mechanical effects,[4] and mechanical degradation[5] of electrodes. However, X-ray tomography is not sensitive to the electrolyte, solid electrolyte interphase (SEI), and internal gas because these species cannot effectively scatter X-rays. Neutron-based characterization methods are sensitive to light elements, such as H and Li, and thus are applied to investigate electrolyte wetting,[6] gas generation,[7] and Li-ion distribution[8] inside cells. Nevertheless, the extremely high cost and inconvenience of neutron-scattering methods limit wide application.

There is an urgent need for inexpensive, convenient, and rapid characterization methods to investigate the electrolyte- and gas-related internal changes inside Li-ion cells, which can impact the safety of practical LIBs. Ultrasonic technology is potentially applicable for such purposes since the transmission of ultrasound is highly sensitive to gas, porosity, and mechanical properties of materials.[9] Some researchers have already found that there are relationships between ultrasonic transmission parameters and battery state of charge as well as state of health.[10–13] Previous works are usually based on fixed-point ultrasonic testing, which cannot probe heterogeneity across an entire Li-ion cell.[14–16] These remarkable works demonstrated the feasibility of using ultrasound to study the internal state of lithium-ion cells. However, fixed-point testing only gives ultrasonic information

Context & Scale

The quality of electrolyte wetting has a significant impact on the electrochemical performance of lithium-ion batteries. However, because of the closed configuration of commercial lithium-ion batteries, it is very difficult to see the quality of wetting with conventional imaging methods, including X-ray CT methods. To address this problem, we used a focused ultrasonic beam to conduct a scan over the battery and demonstrate that ultrasonic transmission imaging can effectively measure the quality of electrolyte wetting. The introduced method is non-destructive, fast, cheap, and applicable to large and thick commercial pouch-type and prismatic cells. It is very sensitive to early-stage electrolyte dry-out or "unwetting" and, thus, can be used to give new insight into the failure mechanism of lithium-ion batteries.

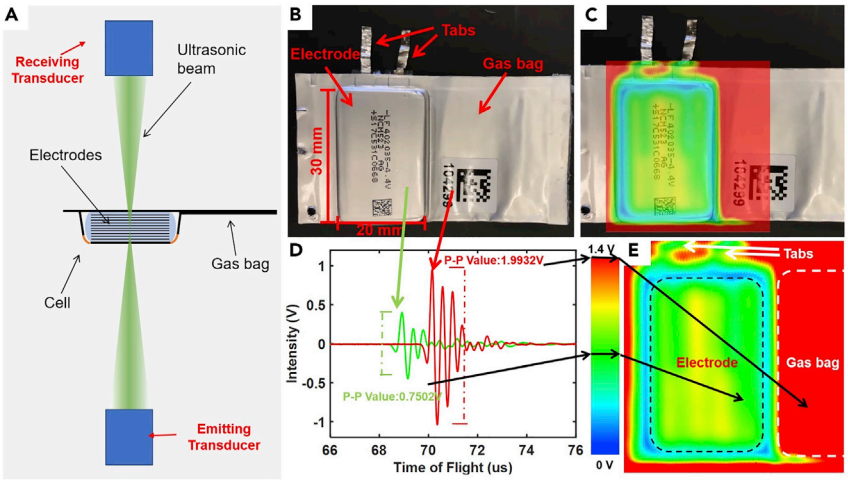

Figure 1. Illustration of the Principle of the Scanning Ultrasonic Instrument

(A) A schematic diagram of the path of the focused ultrasonic beam.

(B) A photograph of a well-wetted NMC532/AG pouch cell used in this study.

(C) The ultrasonic transmission image of the NMC532/AG pouch cell overlapped with its optical photo.

(D) The ultrasonic transmission wave at two points marked with arrows.

(E) The ultrasonic transmission image of the fresh wetted and degassed pouch cell.

averaged over the area covered by the probe. It also cannot probe inhomogeneity within the cell. Robinson et al.[17] measured the ultrasonic properties at multiple positions across a cell and studied the nonuniformity of some structural features. However, such methods still suffer from a substantial lack of spatial resolution because the ultrasonic beam is usually too wide to resolve small structural features.

In this work, we introduce an ultrasonic scanning technique to study pouch and prismatic Li-ion cells. Unlike previous fixed-point measurements, the ultrasound was focused into a thin beam with a diameter less than 1 mm and was scanned with a position control accuracy of 0.2 mm, which yields sub-millimeter resolution, as well as the capability to investigate electrolyte wetting, dry-out, and "unwetting" processes in pouch cells. By "unwetting" we mean that the electrode stack has swelled to such an extent that there is no longer enough electrolyte to completely fill the expanded pore space. The completion of the wetting of a cell electrode stack or "jelly roll" can be clearly observed with this technology. Pouch cells with various electrolyte formulations after cycling at different conditions are also investigated. Gassing, electrolyte dry-out, and/or "unwetting" can be observed in aged cells, which helps to explain their capacity loss after extended testing. The ultrasonic imaging technique developed here is fast and cheap and is applicable to a large pouch or prismatic cells as shown in Figures S1 and S2.

RESULTS AND DISCUSSION

The schematic diagram shown in Figure 1A demonstrates the principle of the ultrasonic scanning method. An ultrasound wave is emitted from the focusing transducer on one side, penetrates the cell, and is received by another transducer on the other side. The transmitted ultrasonic signal is affected by changes in the physical properties of the materials in the path of the focused ultrasonic beam. Figure 1B shows a photo of an NMC 532/artificial graphite (AG) pouch cell. Figure 1D shows the transmitted ultrasonic waves at different positions marked with arrows. The ultrasonic transmission waveform at each position was recorded via progressive scanning. The peak-to-peak value of the

[1]State Key Laboratory of Material Processing and Die & Mould Technology, School of Materials Science and Engineering, Huazhong University of Science and Technology, Wuhan, Hubei 430074, China

[2]Department of Physics and Atmospheric Science, Dalhousie University, Halifax, NS B3H4R2, Canada

[3]HUST - Wuxi Research Institute, Wuxi, Jiangsu 214000, China

[4]State Key Laboratory of Digital Manufacturing Equipment and Technology, School of Mechanical Science and Engineering, Huazhong University of Science and Technology, Wuhan, Hubei 430074, China

[5]Lead Contact

*Correspondence: shenyue1213@hust.edu.cn (Y.S.), huangyh@hust.edu.cn (Y.H.), jeff.dahn@dal.ca (J.R.D.)

https://doi.org/10.1016/j.joule.2020.07.014

ultrasonic transmission wave was transformed into colors from blue to red under the given scale (between 0 and 1.4 V) to create ultrasonic transmission images of the cell. Figure 1C shows the ultrasonic transmission image of an NMC 532/AG pouch cell overlapped with its optical photograph. From the image, we can learn that aluminum-laminate film, as well as the flat gas bag, has relatively high ultrasonic transmissivity. The peak-to-peak value in these red areas is higher than 1.4 V. The multiple layered electrodes and separators reduce the transmission of the ultrasonic wave, and the peak-to-peak value is about 0.75 V, corresponding to a green color. The Al laminate film case of our cells is slightly larger than the electrodes. This causes a small empty gap between the electrode and the case, which heavily attenuates the ultrasonic signal and shows as a light blue ring around the electrode area.

Figure 1 shows that the ultrasonic wave attenuates faster in the well-wetted cell than in the homogeneous medium (empty gas bag). This is because of the reflection and scattering of the ultrasonic wave at the interfaces in the multiple layered porous structures. If the cell is not wetted well, the attenuation of the transmitted ultrasonic signal will be even greater since reflection and scattering at the solid-air interface is much stronger than the solid-solid and solid-liquid interfaces. A pouch cell with a single dry layer was made as shown in Figure 2A. Figure 2B shows the ultrasonic transmission wave from the points marked by arrows inside and outside the dry electrode area. Figure 2C shows the ultrasonic image and Figure 2D shows the ultrasonic image overlapped on the cell photograph for a better understanding. According to Figures 2B and 2C, the peak-to-peak value of the transmitted wave is only 0.0296 V in the region of the dry electrode, indicating that even one layer of the dry electrode can block the majority of the ultrasonic wave.

It is important to stress that the experiments in this paper were made on wound pouch cells with five turns or 10 layers of the double-sided positive electrode and 10 layers of double-sided negative electrode. The variation of the ultrasonic image from scan to scan and from pouch cell to pouch cell is given in Figures S3 and S4. As shown, the peak-to-peak voltage changes caused by wetting or unwetting are much more significant than the variation from scan to scan and cell to cell. Figure S5 shows an ultrasonic image of an NMC532/AG dry pouch cell demonstrating that ultrasound does not pass through the dry pouch cell, even if it is well packed.

Figures 2E and 2F further demonstrate the attenuation mechanism of the ultrasonic wave in the porous electrode. As the ultrasonic wave is a mechanical wave, it needs a medium to propagate. The electrode in the cell can be viewed as closely packed micro-particles. When the electrode is dry, the ultrasonic wave can only transmit by direct contact among the particles. There are a lot of reflections and refractions by these irregular particles, which causes rapid attenuation of the ultrasonic signal. Much of the energy of the ultrasonic wave is consumed by friction between these particles.[9] However, if the electrode is wetted with electrolyte, the electrolyte can serve as a medium for sound waves, providing additional paths for ultrasonic propagation. Therefore, ultrasonic imaging is very sensitive to the wetting status of the LIBs and can be used to study dry-out and "unwetting" in Li-ion cells.

Figure 3 shows the ultrasonic transmission images of NMC532/AG pouch cells filled with different volumes of electrolytes. The blue areas indicate insufficient wetting. Accordingly, wetting homogeneity improves as the volume of electrolyte increases. This pouch cell needs at least 0.8 mL electrolyte to be fully wetted. When the injected electrolyte volume was less than 0.8 mL, at least a portion of one layer of the cell stack was not wetted well. When the injected electrolyte was more than

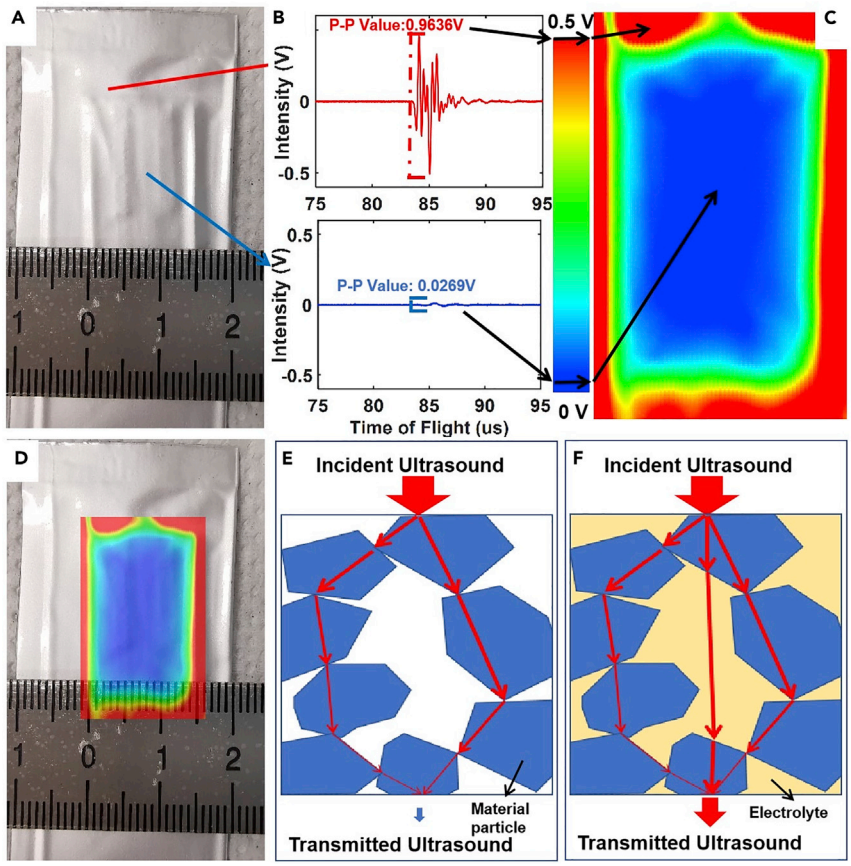

Figure 2. Illustration of How Ultrasonic Waves Are Attentuated When Gas or Vacuum Is between Electrode Particles and How Ultrasonic Wanes Transmit Well When Electrodes Are Well Wetted with Electrolyte.

(A) Photo of a dry single-layer cell.

(B) The ultrasonic transmission waves at the positions marked by arrows.

(C) Ultrasonic transmission image of the dry single-layer cell.

(D) Photo of the dry single-layer pouch cell overlapped with its ultrasonic transmission image.

(E and F) A schematic picture of transmission paths of ultrasonic waves in the porous electrode with (E) and without (F) electrolyte. See also Figure S5.

0.8 mL, there was no significant change in the ultrasonic image, because the cell was already wetted well. Figure 3 also shows extending the wetting time from 4 to 24 h helps improve the wetting quality. Figure S6 shows the detailed waveforms from NMC532/AG pouch cells with 0.7, 0.8, and 1.0 mL of the electrolyte after wetting for 24 h. The peak-to-peak voltage (PPV) of the ultrasonic wave in the well-wetted area is more than 6 times higher than in the insufficiently wetted area.

For a larger cell, the wetting time needs to be longer. Figure 4 shows the time-dependent ultrasonic images of a larger $LiFePO_4$-graphite pouch cell (140 mm × 100 mm) after electrolyte filling. The blue color in the image corresponds to low ultrasonic transmission identifying the insufficiently wetted parts of the cell, while the green color indicates the well-wetted parts. Accordingly, the wetted area spreads from the edge to the center. The majority of the cell was instantly wetted after electrolyte filling, but it took about 34 h to achieve uniform wetting over the whole cell. Insufficient wetting could lead to lithium plating or other undesired reactions if formation is initiated before the completion of wetting. The issue of homogeneous wetting is especially important for the

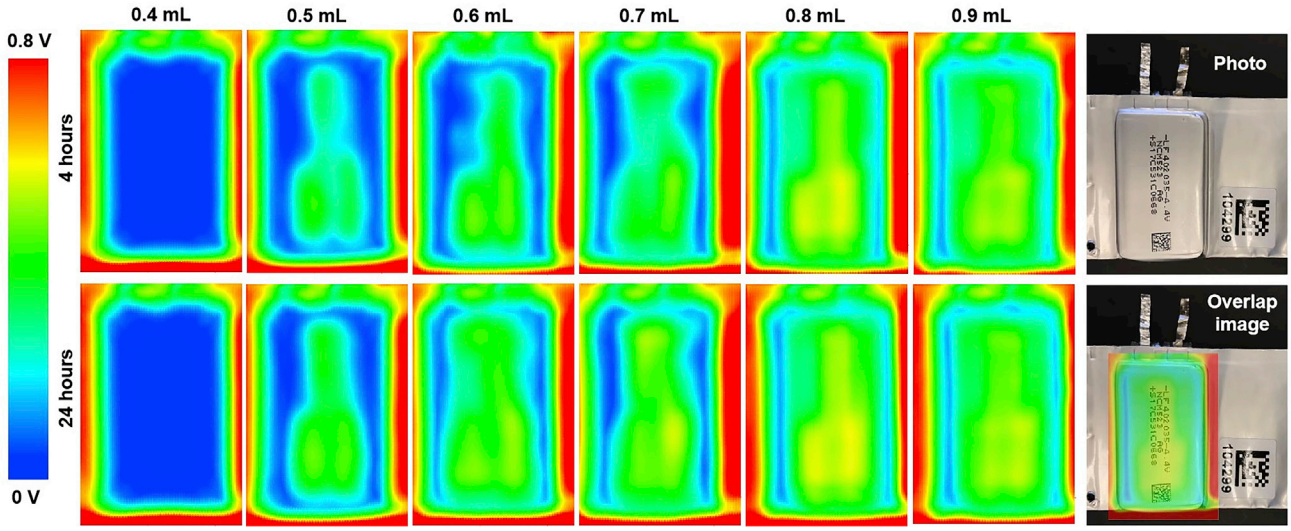

Figure 3. Ultrasonic Images of NMC 532/AG Cells with Different Volumes of Electrolyte after Wetting for 4 and 24 h
See also Figure S6.

preparation of large pouch or prismatic cells. As shown in Figure S2, large commercial cells sometimes suffer very uneven distribution of electrolytes during the initial injection. This kind of uneven distribution creates serious issues associated with lithium plating or other phenomena over cycling, as shown in the ultrasonic images in Figure S2.

Ultrasonic transmission imaging can also be used to study the stability of electrolytes during cycling. Aged cells with different electrolytes and cycling conditions were investigated. Figure 6 shows the ultrasonic transmission images of NMC532/AG pouch cells with electrolyte A, which is a stable electrolyte.[18] The peak-to-peak value of the transmitted ultrasonic signal was converted into color from blue to red. Figures 5A and 5B show that the fresh cell was well-wetted after wetting for 24 h. After formation, some gas was generated. Some gassing reactions during SEI formation are[19–22]:

$$2EC + 2e^- + 2Li^+ \rightarrow (CH_2OCO_2Li)_2 + C_2H_4\ (g)$$

$$EC + 2e^- + 2Li^+ \rightarrow LiOCH_2CH_2OLi + CO\ (g)$$

$$EC + 2e^- + 2Li^+ \rightarrow Li_2CO_3 + C_2H_4\ (g)$$

Ultrasonic waves are very sensitive to gas, even a tiny amount of gas. When ultrasonic waves pass through the interface of two different media, the transmission and reflection ratios can be calculated by formulas 1-1 and 1-2, respectively,[23] where Z_1 and Z_2 are the acoustic impedances of the incident and emergent media, respectively.

$$\text{Transmission rate}: T = \frac{4Z_1 \cdot Z_2}{(Z_1 + Z_2)^2} \qquad 1\text{-}1$$

$$\text{Reflection rate}: R = \frac{(Z_2 - Z_1)^2}{(Z_1 + Z_2)^2} \qquad 1\text{-}2$$

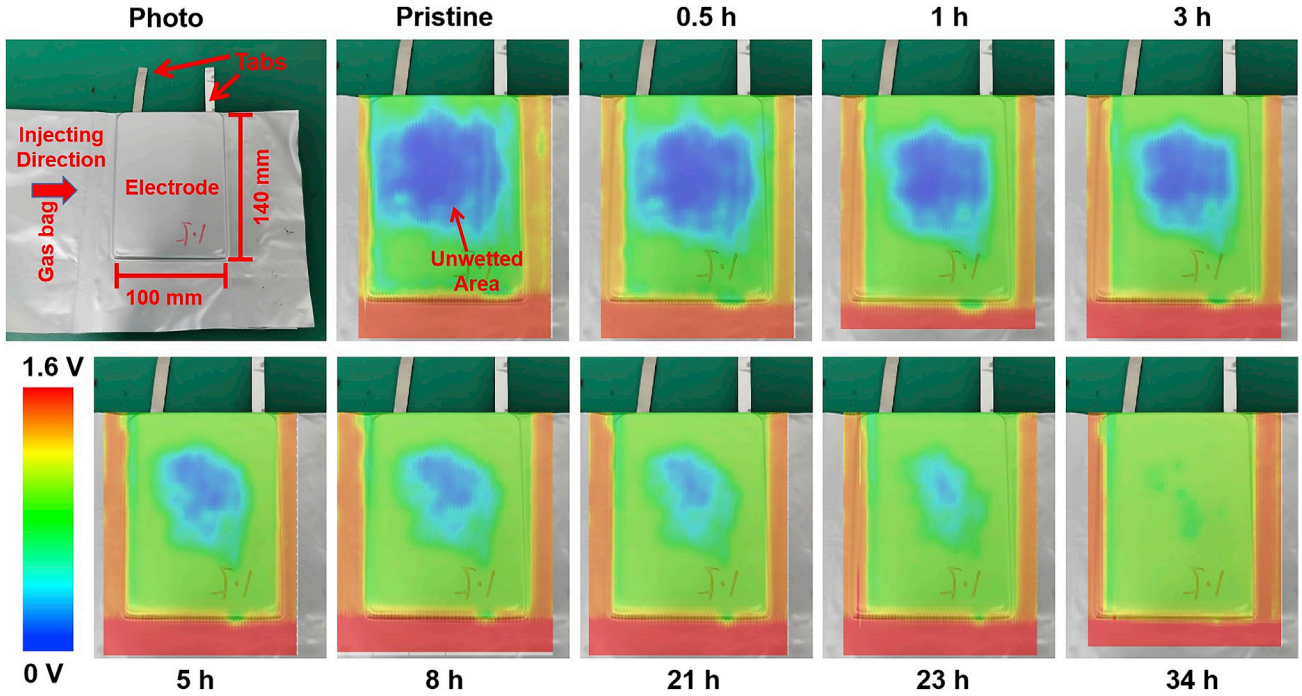

Figure 4. Ultrasonic Images of the Wetting Process of a 100 × 140 mm LiFePO4-Graphite Pouch Cell
The wetting was performed at room temperature.

According to these formulas, similar Z_1 and Z_2 lead to a higher ratio of transmission while different Z_1 and Z_2 lead to a higher ratio of reflection. Usually, the acoustic impedance of gas is near 0.0004 MRayl, and the acoustic impedance of liquid and solid materials are between 1 to 50 MRayl. Such a big difference indicates that ultrasonic waves may lose more than 99.99% of transmitted intensity at the gas/solid interfaces. Therefore, a small amount of gas can drastically lower the ultrasonic transmissivity. Because of the multi-layer structure of these pouch cells, it is difficult to get a quantitative measure of the amount of gas in the cell. For example, if there is severe gassing in two layers, the ultrasound would be blocked by the first layer and hence one cannot detect the gassing in the second layer. However, the ultrasonic method can monitor the early stages of gassing and tell after how many cycles the gassing starts. This can be a useful indicator to compare the stability of electrolytes.

The deep blue area in Figure 5B demonstrates that most of the generated gas accumulated in the gas bag. But there are also some parts of the cell that appear light blue, indicative of a small amount of gas that stayed in the jelly roll region. After degassing, the ultrasonic image of the cell turns to green again (Figure 5C), implying that the gas generated during formation is removed during the degassing step.

After cycling 3,000 times at 20°C, the aged cell in Figure 5D exhibits a similar ultrasonic transmission image to the fresh cell in Figure 5C. There is no blue area in the aged cell, nor in the gas bag, indicating that gassing during cycling is insignificant and that there is no electrolyte dry-out or "unwetting". This result agrees with the excellent capacity retention of the cell (Figure 5E).

Higher temperature leads to more serious electrolyte decomposition and SEI growth. To investigate this process, a group of NMC532/AG pouch cells with

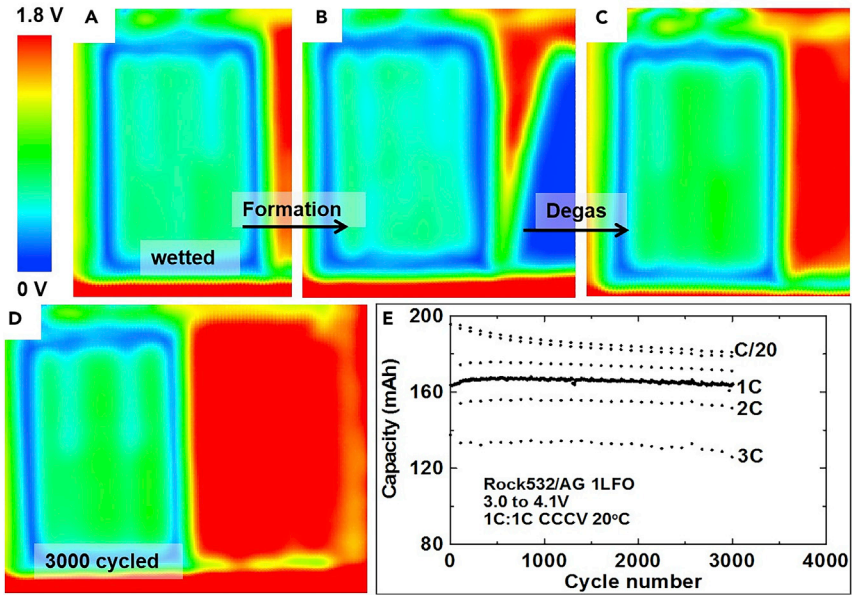

Figure 5. Ultrasonic Images of a Single Crystal NMC532/AG Cell with Electrolyte A
(A) After wetting.
(B) Post formation.
(C) Post degas.
(D) After 3,000 cycles.
(E) Capacity versus cycle number.

electrolyte B were made and cycled with different upper cutoff potentials at 55°C for 2,500 cycles (2 years of continuous cycling at C/3). Figure 6D shows the cells were well-wetted after formation and degassing. After 2,500 cycles in the potential range of 3.0–4.1 V at 55°C, the cell exhibited a large blue area in the ultrasonic transmission image shown in Figure 6E. This phenomenon indicates there is electrolyte dry-out, "unwetting," and/or gassing during cycling. Then, the cell was degassed so that the influence of gas was eliminated. After degassing, there is still some blue area in the image of the cell, which is purely due to electrolyte dry-out or "unwetting". Similar phenomena can also be seen in the cells with 4.2 and 4.3 V cutoff potential.

Figure 6A shows the capacity versus cycle number for each cell tested at 55°C. The continuous decrease in the capacity indicates loss of lithium inventory due to reactions between the negative electrode and the electrolyte. Figure 6B shows the fractional capacity versus cycle number for each cell. Even when cycled to different upper cutoff potentials, the fractional capacity curves of three cells overlap well, which suggests that the three cells had the same aging mode that was shown by Harlow et al.[24] to be lithium inventory loss at 55°C. Figure 6C shows the normalized (to that of cycle 10) difference between the average charge voltage and the average discharge voltage, $\Delta V/\Delta V_{10}$, plotted versus cycle number for each cell. $\Delta V/\Delta V_{10}$ increases about 1.4 times over 2,500 cycles for all cells, so the internal resistance growth of the cells is partially responsible for the capacity loss.[25] In any event, the ultrasonic images in Figure 6 clearly show that, unlike the cell tested at room temperature in Figure 6, the cells tested at 55°C are no longer well wetted after 2 years of testing at 55°C.

To further explore the impact of cycling conditions on the ultrasonic images of aged cells, two NMC622/ natural graphite (NG) cells that had been tested for 2.5 years

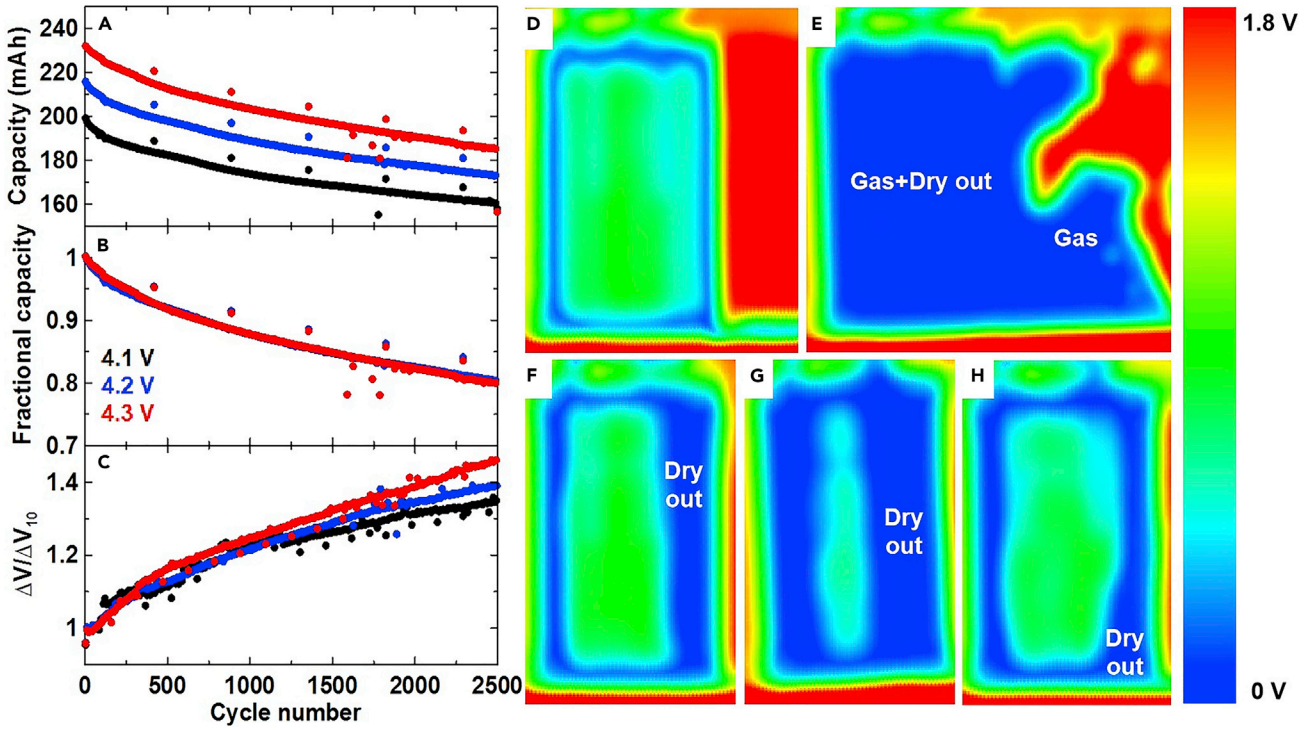

Figure 6. Single Crystal NMC532/AG Cell with Electrolyte B

(A) Capacity versus cycle number.

(B) Fractional capacity versus cycle number.

(C) Fractional polarization voltage versus cycle number.

(D) Ultrasonic image of a fresh cell.

(E) Ultrasonic image of the cell charged to 4.1 V at 55°C for 2,500 cycles before degassing.

(F) Ultrasonic image of the cell in (E) after degassing.

(G) Ultrasonic image after the cell was tested to 4.2 V at 55°C for 2,500 cycles after degassing.

(H) Ultrasonic image after the cell was tested to 4.3 V at 55°C for 2,500 cycles after degassing.

were examined. As shown by Glazier et al.,[26] the natural graphite negative electrodes used in these cells show more swelling during cycling than the artificial graphite used in the cells described by Figures 5 and 6. Figure 7A shows the capacity versus time for the two cells tested at 40°C. One cell was tested at 100% depth of discharge (DOD) between 3.0 and 4.1 V at C/3, while the other was tested between 3.77 and 4.1 V (25% DOD) at C/10. Figure 7A shows that the cell undergoing 25% DOD cycling exhibits less capacity loss than the cell undergoing 100% DOD cycling even though both cells have been tested for the same period of time. This type of behavior for low DOD cycling is well known for Li-ion cells.[27]

In Figure 7A, the cell undergoing 25% DOD cycles has no capacity loss in the 25% DOD cycles, but some capacity loss appears in the 100% DOD check-up cycles performed every 900 h. This is because lithium inventory loss is not observed in 25% DOD cycling. Figure 7B shows the ultrasonic image (after degassing) of the 25% DOD cell, which remains well wetted throughout testing. In Figure 7C, the volume change (before degassing), thickness change, and capacity loss (of the check-up cycles) for the 25% DOD cell are all very minimal even after 2.5 years of testing at 40°C. For the cell tested under 100% DOD conditions, the ultrasonic image (after degassing) in Figure 7D indicates that the cell is no longer completely wetted. Figure 7E shows that the volume change (before degassing), thickness change, and capacity loss (of the check-up cycles) for the 100% DOD cell are relatively large after 2.5 years testing at 40°C.

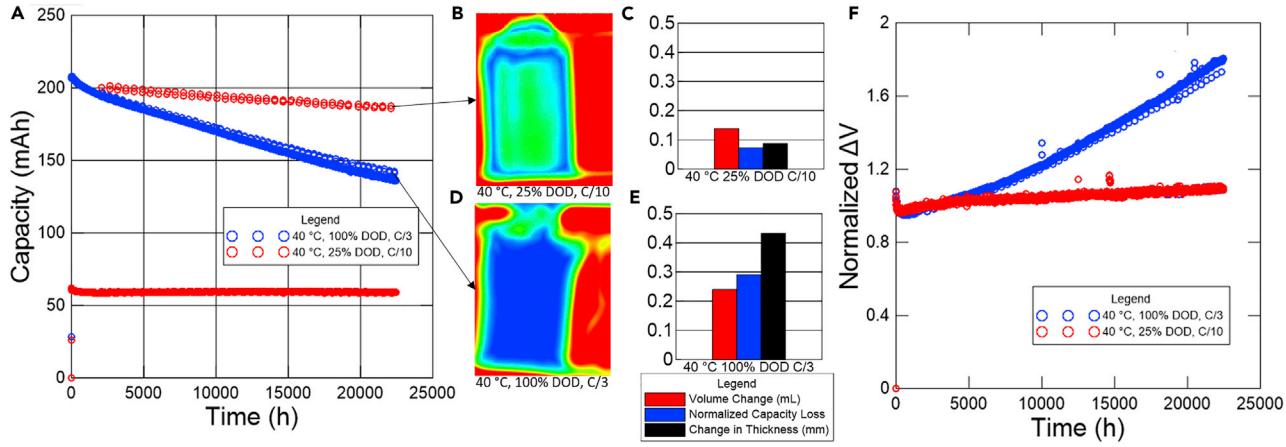

Figure 7. NMC 622/NG Cells Cycled for 2 years

(A) Capacity versus time.

(B) Ultrasonic image of cell with cycling conditions of 40°C, 25% depth of discharge, C/10.

(C) Volume change, normalized capacity loss, and change in thickness for the cell shown in (B).

(D) Ultrasonic image of cell with cycling conditions of 40°C, 100% depth of discharge, C/3.

(E) Volume change, normalized capacity loss, and change in thickness for the cell shown in (D).

(F) Normalized ΔV (average charge voltage minus average discharge voltage) versus time.

Interestingly, the volume change of the cell tested under the 100% DOD condition is exactly equal to that predicted based on the thickness change and the area of the jelly roll (Figure 7E). This suggests that the volume change comes about completely due to swelling of the electrode stack, most likely due to swelling of the natural graphite negative electrode as observed by Glazier et al.[26] Figure 7E shows the volume of the electrode stack has increased by about 0.25 mL, and Figure 3 clearly shows that a shortage of 0.25 mL of electrolyte is sufficient to cause poor ultrasonic transmission. Therefore, we believe that Figures 7D and 7E indicate that the cell tested under 100% DOD conditions is "unwetting," that is, there is no longer enough electrolyte to fill the increased pore space. This is due to the swelling of the natural graphite negative electrode caused by SEI thickening, related to capacity loss. Figure 7F shows normalized ΔV versus cycle time for the two cells. The cell undergoing 100% DOD cycling shows a significant increase in polarization, which is consistent with the explanation given above. We believe that ultrasonic imaging is a very good way to probe "unwetting" in Li-ion pouch and prismatic cells.

Our developed ultrasonic imaging technology is a very useful non-destructive method to characterize the state of electrolyte and/or gas inside a pouch or prismatic cells. Ultrasound attenuates faster in insufficiently wetted electrodes or separators than in well-wetted ones. Ultrasonic transmission imaging can quickly determine the minimum electrolyte injection volume and wetting time, which is helpful to optimize the battery manufacturing process. Gas can also block the transmission of ultrasound. Therefore, this technique can be used to study aged cells and find evidence for electrolyte dry-out or "unwetting" without disassembling the cell. Cells with good electrochemical cycling stability exhibit stable and uniform ultrasonic transmissivity even after thousands of cycles. By contrast, the cells studied here that experienced substantial capacity loss showed poor ultrasonic transmission in parts of the jelly roll or throughout the entire jelly roll. The study on NMC622/NG cells suggests that the poor ultrasonic transmission was caused by an insufficient amount of electrolyte in the cell after negative electrode swelling had occurred, which we call "unwetting" here.

In the future, the scanning speed of the ultrasonic technique can be easily multiplied by increasing the number of ultrasonic transducers. It is possible that dry coupling to the cells can be implemented to avoid the use of liquid coupling as was done here using silicone oil.[28] The application of this ultrasonic cell scanning technique could be extended to online inspections in LIB manufacturing facilities.

EXPERIMENTAL PROCEDURES

Resource Availability

Lead Contact

Jeff. R. Dahn. Correspondence: jeff.dahn@dal.ca

Materials Availability

The study did not generate new unique reagents.

Data and Code Availability

All data needed to evaluate the conclusions in the paper are present in the paper or Supplemental Information.

Ultrasonic Imaging

The ultrasonic images were obtained from an ultrasonic battery scanner (UBSC-LD50 from Jiangsu Jitri-Hust Intelligent Equipment Technology Co., Ltd) shown in Figure S7A. Pouch cells in this work were mounted by their tabs on a battery testing clamp. A pair of ultrasonic focusing transducers (2 MHz frequency, 30 mm focal distance, focusing diameter <1 mm, customized from Shantou Institute of Ultrasonic Instruments Co., Ltd.) were positioned one on each side of the pouch cell as shown in Figure S7B. Transducers and cells were immersed in low-viscosity silicone oil (PSF-10cSt from Clearco Products Co. Inc.), an ultrasonic coupling agent. The transducers were installed on a 2-dimensional motion system with a precision of 0.2 mm so that scanning and imaging could be performed. For the 20 × 30 mm cell scanned with a precision of 0.2 mm in our experiments, it takes about 5 min for one scan. The driving source used in this work was a 200 V pulse signal with a pulse width of 250 ns, matching well with the 2 MHz ultrasonic transducers we used. The average power of the ultrasonic transducer is 25 mW. The waveform of the transmitted signal was recorded with a data collecting card. The peak-to-peak values (P-P value) of received transmitted waves were converted into a color scale to make the pseudo color image. A resolution test (Figures S7C and S7D) shows that sub-millimeter resolution is achieved with this set up.

Cell Specifications

To study the electrolyte wetting, dry-out, and "unwetting" processes, both $LiNi_{0.5}Mn_{0.3}Co_{0.2}O_2$ (NMC532)/AG and $LiNi_{0.6}Mn_{0.2}Co_{0.2}O_2$ (NMC622)/NG dry pouch cells were wetted and cycled in different electrolytes. The cells were 402035 in size with a nominal capacity of about 240 mAh. The dry cells (without electrolyte) were purchased from Li-Fun Technology Ltd., Hunan, China. The pouch cells have a rolled electrode design with 10 layers of the separator/negative/separator/positive stack. The length and width of the jelly roll was 30 × 20 mm and its thickness was about 3 mm. Before being filled with electrolyte, all the cells were dried in vacuum at 80°C for 14 h before being transferred into an Ar-filled glove box.

Electrolyte Preparation

Two different electrolytes were injected into the NMC532/AG pouch cells.

Electrolyte A: 1.2 M $LiPF_6$ in ethylene carbonate(EC): ethyl methyl carbonate (EMC): dimethyl carbonate (DMC) (25:5:70 wt % ratio) electrolyte with 1 wt % $LiPO_2F_2$ (LFO).

Electrolyte B: 1.2 M $LiPF_6$ in EC:EMC (30:70 wt % ratio) electrolyte with 2 wt % vinylene carbonate (VC) and 1 wt % ethylene sulfate (DTD).

The electrolyte used in the NMC622/NG cells was 1.0 M $LiPF_6$ in EC:EMC 3:7 with additives of 2 wt % VC (BASF, 99.5%, < 100 ppm water), 1 wt % tris(trimethylsilyl) phosphite(TTSPi) (Tokyo Chemical Industry Co., Ltd. (TCI), >95.0%), and 1 wt % methylene methanedisulfonate(MMDS) (Guangzhou Tinci Co. Ltd, 98.70%).

Wetting Experiments

In the wetting experiment, a series of volumes of electrolyte A from 0.4 to 1.0 mL with an interval of 0.1 mL were filled into NMC532/AG pouch cells in a glovebox. Then the cells were sealed under -90 kPa gauge pressure. Cells were held at 1.5 V to avoid the dissolution of copper foil.

Handmade LiFePO4-graphite pouch cells with larger size (100 × 140 mm) were also used to study the wetting process. First, an Al laminated film pouch cell case was made with a punching machine (Model MSK-120 from MTI Corp.). Then, the $LiFePO_4$ and graphite electrodes, which were purchased from Kejing Material Technology Co., were cut into the desired size with an Electrode Sheet Punching Machine (Model MSK-180 from MTI Corp.). After that, $LiFePO_4$ electrodes and graphite electrodes were stacked into a special mold one by one and separated by separator membranes. Tabs were connected to the electrodes by an Ultrasonic Welder (Model MSK-800 from MTI Corp.). The electrode stack with tabs was put into the pouch cell case, followed by heat sealing three sides of the case. All the steps above were performed in a "dry" room with a relative humidity lower than 15%. The semi-finished cells were transferred into an Ar-filled glove box. Electrolyte composed of 1.0 M $LiPF_6$ in EC:DMC:EMC = 1:1:1 wt % ratio was used to wet the cell. The last side of the cell was sealed using a Vacuum Sealing Machine (Model MSK-115 from MTI Corp.) after electrolyte injection. Ultrasonic images were collected at different times after the electrolyte filling to monitor the homogeneity of the wetting versus time.

Cycling Experiments

In the first cycling experiment, NMC532/AG pouch cells with 0.85 mL electrolyte A were cycled between 3.0 and 4.1 V at 20°C. For the first 100 cycles, they were charged and discharged at 1 C rate. The charge was 4.1 V followed by a constant voltage step (CCCV) until the current decreased to C/20. After 100 cycles at 1 C, rate performance tests with C/20, C/2, 1 C, 2 C, and 3 C rate discharge currents were run in the next 5 cycles. This cycle mode was repeated till 3,000 cycles were completed.

In the second cycling experiment, NMC532/AG pouch cells with 0.85 mL electrolyte B were cycled between 3.0 and 4.1, 4.2, or 4.3 V at 55°C. The cells were cycled with C/3 charge and discharge rates with a CCCV step applied to a limiting current of C/20 at the upper cutoff potential. Cells were cycled 2,500 times for about 2 years. A group of new cells with the same electrolyte and manufacturing steps as the aged cells were created as a comparator group.

In the third cycling experiment, NMC622/NG cells were tested at 40°C. One cell was cycled between 3.0 and 4.1 V at C/3 (CCCV to C/20 at 4.1 V) while the other was

cycled between 3.77 and 4.1 V, corresponding to 25% DOD at C/10 (based on the full cell capacity). These cells were cycled for 23,000 h, which corresponds to about 2.5 years. Every 900 h the cell testing at 25% DOD was given one full cycle between 3.0 and 4.1 V as a capacity check-up cycle.

SUPPLEMENTAL INFORMATION

Supplemental Information can be found online at https://doi.org/10.1016/j.joule.2020.07.014.

ACKNOWLEDGMENTS

The authors from Huazhong University of Science and Technology were supported by the National Key R&D Program of China (grant no. 2018YFB0905400) and National Natural Science Foundation of China (grant nos. 51672098, 51632001). The Dalhousie authors acknowledge funding under the auspices of the NSERC/Tesla Canada Industrial Research Chair Program.

AUTHOR CONTRIBUTIONS

Z.D. helped design and build the instrument, wrote software to control the instrument, performed many ultrasonic measurements on cells reported, and wrote the first draft of the paper. H.Z.Y. wrote the underlying control program for the instrument. H.D. provided guidance for instrument design and manufacturing. Y.S. and Y.H.H. supervised the experiments made in China. A.L. and M.J. performed ultrasonic measurements in Canada, and M.J. made some modifications to the instrument. R.G. and J.E.H. provided the long-term tested cells (>2 years) that were used for ultrasonic measurements. J.R.D. oversaw and directed experiments in Canada and extensively modified the paper after the first draft. All co-authors provided comments on the manuscript at various stages.

DECLARATION OF INTERESTS

Z.H., Y.S., and Y.H. are employees of Jiangsu Jitri-Hust Intelligent Equipment Technology. H.D. is a founder of Jiangsu Jitri-Hust Intelligent Equipment Technology. Z.D., Y.S., and Y.H. are the inventors of patents CN201811075406.0 (In application), CN201820907470.X, and CN201810602231.8. The authors declare no other competing interests.

Received: April 16, 2020
Revised: June 2, 2020
Accepted: July 14, 2020
Published: August 12, 2020

REFERENCES

1. Goodenough, J.B., and Kim, Y. (2010). Challenges for rechargeable Li batteries. Chem. Mater. *22*, 587–603.

2. Eastwood, D.S., Bayley, P.M., Chang, H.J., Taiwo, O.O., Vila-Comamala, J., Brett, D.J., Rau, C., Withers, P.J., Shearing, P.R., Grey, C.P., and Lee, P.D. (2015). Three-dimensional characterization of electrodeposited lithium microstructures using synchrotron X-ray phase contrast imaging. Chem. Commun. (Camb.) *51*, 266–268.

3. Lim, C., Yan, B., Yin, L., and Zhu, L. (2012). Simulation of diffusion-induced stress using reconstructed electrodes particle structures generated by micro/nano-CT. Electrochim. Acta *75*, 279–287.

4. Finegan, D.P., Scheel, M., Robinson, J.B., Tjaden, B., Hunt, I., Mason, T.J., Millichamp, J., Di Michiel, M., Offer, G.J., Hinds, G., et al. (2015). In-operando high-speed tomography of lithium-ion batteries during thermal runaway. Nat. Commun. *6*, 6924.

5. Müller, S., Pietsch, P., Brandt, B.E., Baade, P., De Andrade, V., De Carlo, F., and Wood, V. (2018). Quantification and modeling of mechanical degradation in lithium-ion batteries based on nanoscale imaging. Nat. Commun. *9*, 2340.

6. Weydanz, W.J., Reisenweber, H., Gottschalk, A., Schulz, M., Knoche, T., Reinhart, G., Masuch, M., Franke, J., and Gilles, R. (2018). Visualization of electrolyte filling process and influence of vacuum during filling for hard case prismatic lithium ion cells by neutron imaging to optimize the production process. J. Power Sources *380*, 126–134.

7. Michalak, B., Sommer, H., Mannes, D., Kaestner, A., Brezesinski, T., and Janek, J. (2015). Gas evolution in operating lithium-ion batteries studied in situ by neutron imaging. Sci. Rep. *5*, 15627.

8. Siegel, J.B., Lin, X., Stefanopoulou, A.G., Hussey, D.S., Jacobson, D.L., and Gorsich, D. (2011). Neutron imaging of lithium concentration in LFP pouch cell battery. J. Electrochem. Soc. *158*, A523.

9. Schmerr, L.W. (2016). Fundamentals of Ultrasonic Non-destructive Evaluation (Springer).

10. Hsieh, A.G., Bhadra, S., Hertzberg, B.J., Gjeltema, P.J., Goy, A., Fleischer, J.W., and Steingart, D.A. (2015). Electrochemical-acoustic time of flight: in operando correlation of physical dynamics with battery charge and health. Energy Environ. Sci. *8*, 1569–1577.

11. Ladpli, P., Kopsaftopoulos, F., Nardari, R., and Chang, F.-K. (2017). Battery charge and health state monitoring via ultrasonic guided-wave-based methods using built-in piezoelectric transducers. Smart Materials and Non-destructive Evaluation for Energy Systems 2017 (International Society for Optics and Photonics), p. 1017108.

12. Gold, L., Bach, T., Virsik, W., Schmitt, A., Müller, J., Staab, T.E.M., and Sextl, G. (2017). Probing lithium-ion batteries' state-of-charge using ultrasonic transmission – concept and laboratory testing. J. Power Sources *343*, 536–544.

13. Schmidt, R.D., and Sakamoto, J. (2016). In-situ, non-destructive acoustic characterization of solid state electrolyte cells. J. Power Sources *324*, 126–133.

14. Gaponov, V., Kuznetsov, D., Dudnik, V., and Afanasieva, N. (2018). Ultrasound method of Li-ion electric battery monitoring. In International Conference "actual Issues of Mechanical Engineering, pp. 145–149.

15. Knehr, K.W., Hodson, T., Bommier, C., Davies, G., Kim, A., and Steingart, D.A. (2018). Understanding full-cell evolution and non-chemical electrode crosstalk of Li-Ion batteries. Joule *2*, 1146–1159.

16. Chang, W., Bommier, C., Fair, T., Yeung, J., Patil, S., and Steingart, D. (2020). Understanding adverse effects of temperature shifts on Li-Ion batteries: an operando acoustic study. J. Electrochem. Soc. *167*, 090503.

17. Robinson, J.B., Maier, M., Alster, G., Compton, T., Brett, D.J.L., and Shearing, P.R. (2019). Spatially resolved ultrasound diagnostics of Li-ion battery electrodes. Phys. Chem. Chem. Phys. *21*, 6354–6361.

18. Ma, L., Ellis, L., Glazier, S.L., Ma, X., Liu, Q., Li, J., and Dahn, J.R. (2018). $LiPo_2F_2$ as an electrolyte additive in $Li[Ni_{0.5}Mn_{0.3}Co_{0.2}]O_2$ /graphite pouch cells. J. Electrochem. Soc. *165*, A891–A899.

19. Arakawa, M., and Yamaki, J. (1995). Anodic oxidation of propylene carbonate and ethylene carbonate on graphite electrodes. J. Power Sources *54*, 250–254.

20. Schechter, A., Aurbach, D., and Cohen, H. (1999). X-ray photoelectron spectroscopy study of surface films formed on Li electrodes freshly prepared in alkyl carbonate solutions. Langmuir *15*, 3334–3342.

21. Aurbach, D. (2000). Review of selected electrode–solution interactions which determine the performance of Li and Li ion batteries. J. Power Sources *89*, 206–218.

22. An, S.J., Li, J., Daniel, C., Mohanty, D., Nagpure, S., and Wood, D.L., III (2016). The state of understanding of the lithium-ion-battery graphite solid electrolyte interphase (SEI) and its relationship to formation cycling. Carbon *105*, 52–76.

23. Kinsler, L.E., Frey, A.R., Coppens, A.B., and Sanders, J.V. (1999). Fundamentals of Acoustics, 4th Edition (Wiley-VCH).

24. Harlow, J.E., Ma, X., Li, J., Logan, E., Liu, Y., Zhang, N., Ma, L., Glazier, S.L., Cormier, M.M.E., Genovese, M., et al. (2019). A wide range of testing results on an excellent lithium-ion cell chemistry to be used as benchmarks for new battery technologies. J. Electrochem. Soc. *166*, A3031–A3044.

25. Arora, P. (1998). Capacity fade mechanisms and side reactions in lithium-ion batteries. J. Electrochem. Soc. *145*, 3647.

26. Glazier, S.L., Li, J., Louli, A.J., Allen, J.P., and Dahn, J.R. (2017). An analysis of artificial and natural graphite in lithium ion pouch cells using ultra-high precision coulometry, isothermal microcalorimetry, gas evolution, long term cycling and pressure measurements. J. Electrochem. Soc. *164*, A3545–A3555.

27. Deshpande, R.D., and Bernardi, D.M. (2017). Modeling solid-electrolyte interphase (SEI) fracture: coupled mechanical/chemical degradation of the lithium ion battery. J. Electrochem. Soc. *164*, A461–A474.

28. Komsky, I.N. (2005). Transmission of longitudinal and transverse ultrasonic waves using dry-coupled transducer modules. AIP Conf. Proc. *760*, 1010–1017.